Nonlinear Adsorption Characteristics Of Lithium At The Cape Cod Tracer Test

Neal T. Graham

A scholarly paper in partial fulfillment of the requirements for the degree of

Master of Science

May 2016

Department of Atmospheric and Oceanic Science, University of Maryland
College Park, Maryland

Advisor: Dr. Fernando Miralles-Wilhelm

Table of Contents

Abstract

Contaminants within groundwater move in the subsurface depending upon the physical and chemical nature of the contaminant and the physical and chemical characteristics of the aquifer in which the groundwater is located. In this study, nontoxic amounts of the nonlinear adsorbing solute lithium was traced over a three-year period in a sand and gravel aquifer, which has had both chemical and physical characteristics documented in previous studies, located in Cape Cod, Massachusetts. The lithium data is compiled into spatial moment representations, using a trapezoidal integration technique along with a Delaunay triangulation scheme, in order to quantify plume characteristics throughout the experiment. Comparisons are made between the results of this study to that of a study completed in 1987, which used slightly different methods to quantify the data over time. Quantitative sets of equations are then derived using a Gaussian Plume model approximation as well as a Saturated flow approximation in order to attempt to model the spatial moment changes over time. Results are shown for the derived spatial moment equations and the results of the comparison between model and field data.

Acknowledgements

I would like to take this opportunity to thank my mother for always being by my side throughout my entire academic career, my wife Ashley for taking this leap of faith with me and for consistently being my rock through all the stress and successes that have come thus far in my academic career, my friends that I have made at all stages of this journey, whether it be grade school, or Rutgers, or Maryland, and my advisor Fernando, for providing the assistance and guidance needed to reach this point in my career and for the opportunities that he has allowed me to take advantage of in the short time of my life that I have known him.

List of Tables

List of Figures

List of Symbols

S – Amount of mass adsorbed to soil pores

K_F – Freundlich Adsorption Isotherm

C – Mass of solute in solution

N – Adsorption Coefficient

q_i – Velocity of groundwater in (x,y,z) direction

K_{ij} – Hydraulic Conductivity of Aquifier

dh/dx_j – Pressure Gradient Force

D_{ij} – Diffusivity in (x,y,z) direction

I_n – Vertically Integrated Concentration

$x_{(a,b,c)}$ – One of three points on a triangle in the x-y plane

M_k – Spatial Moment dependent upon value of k

k – Value used to specify spatial moment (0,1,2,3)

n – porosity of aquifer

x_i – Location in (x,y,z) direction

ρ_b – Bulk density of soil

M_s – Mass adsorbed

M_T – Total Mass

$V_{(x,y,z)}$ – Velocity in (x,y,z) direction

t - time

Chapter 1: Introduction

1.1 Preface

As groundwater moves in the subsurface, contaminants within the water can adsorb to soil pores based upon both the physical and chemical properties of the aquifer in which the groundwater is located. The rate at which sorption, the process by which a material adsorbs to soil pores, is typically represented by an adsorption isotherm determined through laboratory experiments (Buergisser et al, 1993). These isotherms describe the amount of solute sorbed to the total amount in concentration at a constant temperature. Adsorption isotherms can be both linear and nonlinear in nature depending upon the chemical nature of the adsorbent. For the purpose of this experiment, the structure of a Freundlich isotherm (Freundlich 1906) has been assumed based on a previous study (Garabedian 1987). The adsorption isotherm used during this experiment can be seen in Equation 1.1 where S is the mass sorbed, K_F is the Freundlich coefficient, C is the mass in solution, and N is the adsorption coefficient.

$$S = K_F C^N \tag{1.1}$$

Quantitative models are used in science today to predict everything from the weather to population based income changes; subsurface hydrology can also make use of these models. In this experiment, a large-scale natural gradient tracer test is analyzed in an effort to model the nonlinear movement and decay of a controlled contaminant injected into the soil. Field data collected throughout the duration of the test, described in section 1.2, is analyzed and compared to a numerical model derived to test the lifetime changes of contaminants injected during the tracer test

and the reliability of the quantitative model. Calculations from data collected in the field are made of total change of mass, the location of the center of mass over time, and the variance of the contamination plume around the center of mass. The calculated values are then compared to a previous study that calculated the same values using a different technique. Using the quantitative model, described in section 2.2, attempts are made at predicting changes in the plume characteristics over time. Finally, concluding remarks are made and suggestions for future work and improvements are provided.

1.2 Test Description

A large-scale tracer test was conducted over a three-year period beginning in July 1985, in which three chemical contaminant solutions were injected as a pulse at a source location and the three-dimensional transport and dispersion of the contamination plumes were monitored. These contaminant solutions contained nontoxic amounts of bromide, a nonreactive tracer, lithium and molybdenum, both reactive tracers (LeBlanc et al. 1991). This paper will look at the transport and dispersion of the lithium plume in order to gain a better understanding of the processes controlling nonlinear adsorption. Through lab experiments, it has been shown that solutions containing lithium compounds adsorb to soil pores nonlinearly during subsurface groundwater movement (Stollenwerk and Kim, 1990; Wood et al. 1990). While lithium solutions undergo sorption, solutions containing bromide move linearly through the subsurface while not adsorbing to the soil and thus act as quality groundwater tracers (Garabedian 1987). For the purposes of this

experiment, the bromide data will be used to estimate the total groundwater velocity and as a movement comparison to the lithium plume.

The tracer test was completed on the western part of Cape Cod, Massachusetts, near Otis Air Base, at an abandoned gravel pit in which the experimental groundwater plume could remain unobstructed throughout the duration of the experiment. The location of the site can be seen in Figure 1 below in which the hatched area represents the test site and the dashed line is the water table altitude in meters. Known concentrations of the bromide, lithium, and molybdenum solutions were injected at a single injection site during a 24-hour period. Bore holes were dug south and east of the injection sites, as seen in Figure 2, where concentration measurements could be made at multiple levels, shown in Figure 3, throughout the hole. A comprehensive description of the test site and measuring techniques can be found in Leblanc et al. 1991.

Figure 1, From Leblanc et al. 1991

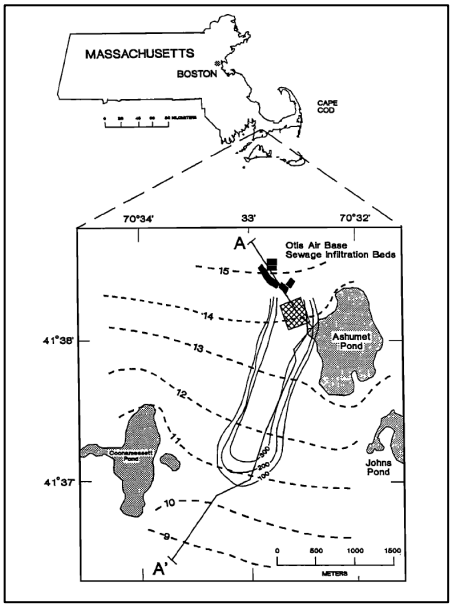

Figure 2, From Leblanc et al. 1991

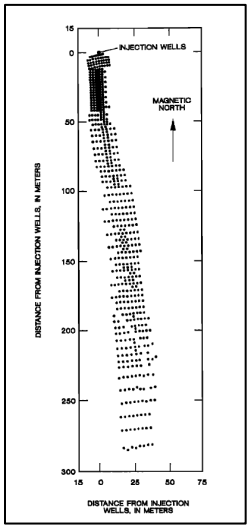

Figure 3, From Leblanc et al. 1991

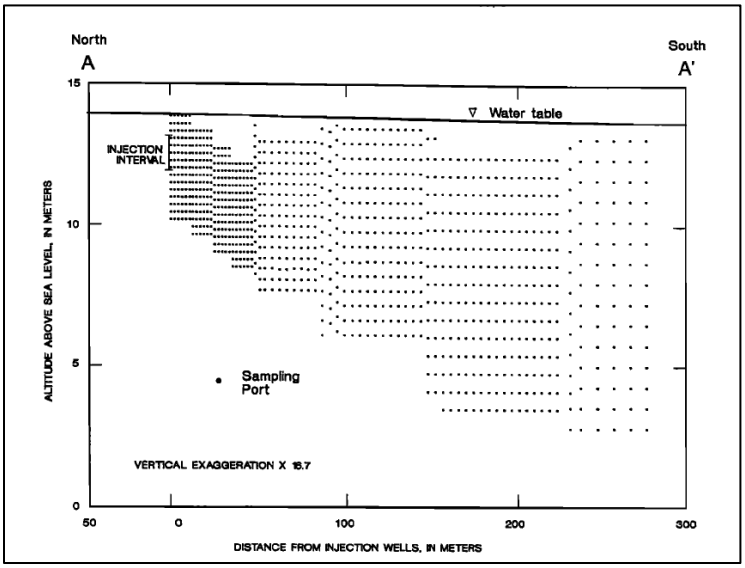

1.3 Groundwater Movement Kinetics

The movement of water in the subsurface has several driving forces that determine the ability to flow and the flow rate of groundwater. The hydraulic conductivity, or the permeability of the aquifer, is often highly spatially variable within a single aquifer (Gelhar 1993)(Sudicky, 1986). The spatial variability of the

hydraulic conductivity arises from large heterogeneities within an aquifer. These heterogeneities can be physical in nature, such as changes between sand and gravel, or they can be chemical in nature, such as having different sorption properties. In this study an aquifer-wide estimated hydraulic conductivity was used (LeBlanc et al. 1991). Along with an aquifer-wide hydraulic conductivity, aquifer scale porosity has been calculated to determine the amount of void space within the aquifer (Garabedian 1991). The movement of groundwater is based upon Darcy's Law and Fick's Law.

$$q_i = -K_{ij}\left(\frac{dh}{dx_j}\right) \tag{1.2}$$

$$J_i = -D_{ij}\left(\frac{dc}{dx_j}\right) \tag{1.3}$$

Darcy's Law, Equation 1.2, describes the flow rate, q_i, of a fluid though a porous medium depending upon the hydraulic conductivity, K_{ij}, and pressure gradient, (dh/dx_j), present in the medium. Fick's Law represents the diffusion, D_{ij}, of a substance, (dc/dx_j), over time in a particular direction. This study assumes a fully saturated flow pattern throughout the duration of the test; therefore all equations presented are shown in terms of saturated flow.

1.4 Moment Definition

Three-dimensional representations for groundwater plume characteristics can be defined by spatial moments. Spatial moments define characteristics of groundwater plumes such as, total mass in solution (zeroth moment), center of mass (first moment), variance about the center of mass (second moment), and

skewness of the groundwater plume (third moment). Changes in spatial moments over time represent the movement characteristics of a groundwater plume. For a sorbing solute such as lithium, over time the zeroth moment decreases in time as mass sorbs to soil pores. The first moment increases at a slower rate than a non-sorbing material as retardation typically occurs due to the sorbing process, which slows the overall movement of the plume. Finally the second moment increases at a faster rate due to the sorption process increasing the spread of the plume. Examples of these can be seen in Figure 4, which illustrates three comparisons between bromide, on the right, and lithium, on the left, during the tracer test. The lithium plume spreads over the direction of flow during the test, while the bromide plume remains in a concentrated ball as it moves with the groundwater. The movement speed can also be seen to be much slower within the lithium plume as the sorption process is occurring, whereas the bromide plume is located nearly 200 feet ahead of the lithium plume after 461 days of the test.

Figure 4.

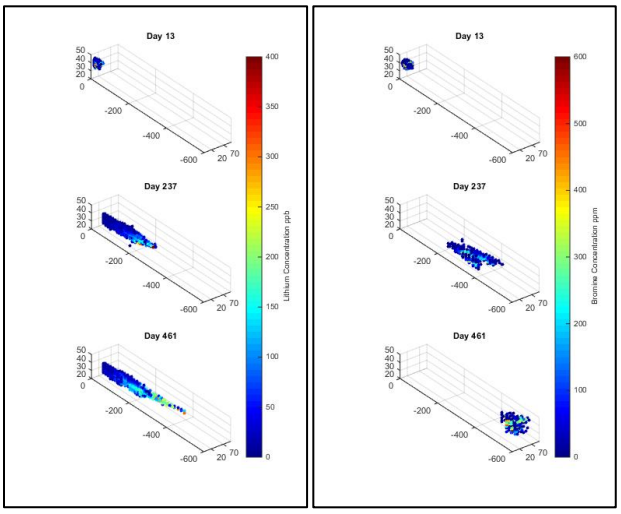

Chapter 2: Methodology

2.1 Moment Calculations of Field Data

Using the Lithium concentrations taken over the duration of the tracer test, the spatial moments can be calculated by using a trapezoidal integration scheme, which will be applicable to all spatial moments with slight exponential variations for higher order moments. This was applied at all unique points within a Cartesian coordinate system using Equation 2.1 below where Z represents the z-coordinate of each unique point and the associated concentration of solute at each point and the exponent n represents the moment being calculated (0,1,2,3).

$$I_n = (Z_2 - Z_1) * \frac{1}{2}[(concentration_1 * Z^n{}_1) + (concentration_2 * Z^n{}_2) \quad (2.4)$$

Once all of the integrals have been calculated we are left with an irregular gridded data set in which a particular point gives the vertical concentration. In order to calculate the total concentration we must apply a grid to the data and find the area of the grid. Due to the irregularity of the points, a Delaunay triangulation approach was used to create the three-dimensional mesh. Delaunay triangulation is process by which a surface of triangles is created in either two or three-dimensional space with a given set of points (Delaunay, 1934). A two-dimensional Delaunay triangulation ensures that the circumcircle associated with each triangle created contains no other point in its interior. With a mesh grid making up the new "surface" of the concentrations we can now find the area of each triangle using the shoelace formula for finding the area of a triangle in an x-y plane as seen in Equation 2.2.

$$area = \frac{1}{2}|(x_a - x_c)(y_b - y_a) - (x_a - x_b)(y_c - y_a)| \quad (2.5)$$

Multiplying the area of each triangle by the average concentration (I_n) of each vertex and summing over the entire mesh results in the value for the specific spatial moment being calculated in a non-porous media. Multiplying by the porosity of the aquifer, in this case 0.39, results in the final spatial moment.

2.2 Mathematical Moment Derivations

Creating a quantitative model for nonlinear moment analysis makes use of several governing equations. The use of these governing equations allows for a reasonable starting point in order to eventually derive quantitative relationships to the time sensitive rates of changes of several spatial moments. The following derivation takes a look at the solute transport equation and its transformation to spatial moment analysis, as well as the governing equation for a solute undergoing nonlinear sorption. The derivation follows closely with derivations completed during a previous study (Miralles-Wilhelm 1993).

2.2.1 Manipulation of the Solute Transport Equation (Zeroth Moment)

Equation 2.3 represents the governing equation for spatial moments for a groundwater plume undergoing nonlinear sorption. The coefficients i and k represent the (x,y,z) coordinate and the specific spatial moment being solved respectively.

$$M_K(t) = \iiint_{-\infty}^{\infty} n\, x_i{}^k C(x,y,z,t)\,dx\,dy\,dz \qquad where\ i = 1,2,3\ and\ k = 0,1,2,3 \tag{2.6}$$

From the governing equation the general form of the zeroth, first, and second spatial moments can be defined below. Similar expressions can be made for spatial moments in the y and z directions.

$$M_0(t) = \iiint_{-\infty}^{\infty} n\, C(x,y,z,t)dxdydz \tag{2.7}$$

$$M_{1x}(t) = \iiint_{-\infty}^{\infty} n\, x\; C(x,y,z,t)dxdydz \tag{2.8}$$

$$M_{2x}(t) = \iiint_{-\infty}^{\infty} n\, x^2\, C(x,y,z,t)dxdydz \tag{2.9}$$

Solute transport for nonlinear sorption can be represented by a second governing equation.

$$x_i{}^k \frac{\partial}{\partial t}(nC + \rho_b S) = -x_i{}^k \frac{\partial}{\partial x_i}(q_i C) + x_i{}^k \frac{\partial}{\partial x_i}[D_{ij} \frac{\partial C}{\partial x_j}] \tag{2.10}$$

The solute transport equation can now be integrated through space with k=0 in order to obtain the solute transport for the zeroth moment definition.

$$\iiint_{-\infty}^{\infty} \frac{\partial}{\partial t}(nC)dxdydz = \frac{\partial}{\partial t}\iiint_{-\infty}^{\infty} nC\; dxdydz \quad but\; M_0 = \iiint_{-\infty}^{\infty} nC\; dxdydz\; so \tag{2.8.1}$$

$$= \frac{\partial M_0}{\partial t} = \frac{dM_0}{dt}$$

$$\iiint_{-\infty}^{\infty} \frac{\partial}{\partial t}(\rho_b S)dxdydz = \frac{\partial}{\partial t}\iiint_{-\infty}^{\infty} \rho_b S\; dxdydz \quad but\; M_S = \iiint_{-\infty}^{\infty} \rho_b S\; dxdydz\; so \tag{2.8.2}$$

$$= \frac{\partial M_S}{\partial t} = \frac{dM_S}{dt}$$

$$\iiint_{-\infty}^{\infty} \left(-\frac{\partial}{\partial x_i}(q_x C) + \frac{\partial}{\partial x}[D_{ij}\frac{\partial C}{\partial x}] \right) dxdydz \tag{2.8.3}$$

$$= -\iint_{-\infty}^{\infty} [-xC]_{-\infty}^{\infty} dydz + \iint_{-\infty}^{\infty} \left[D_{ij}\frac{\partial C}{\partial x} \right] dydz = 0$$

The resulting equation leads to the general understanding that the total mass is the combination of the amount still in solution and the amount that has undergone sorption.

$$\frac{dM_0}{dt} + \frac{dM_S}{dt} = 0 \; or \; M_0 + M_S = M_T \tag{2.9}$$

2.2.2 Manipulation of the Solute Transport Equation (First Moment)

Following the same procedure as before, the solute transport equation can be manipulated to obtain the transport for the first spatial moment definition.

$$x\frac{\partial}{\partial t}(nC + \rho_b S) = -x\frac{\partial}{\partial x_i}(q_i C) + x\frac{\partial}{\partial x_i}[D_{ij}\frac{\partial C}{\partial x}] \tag{2.10}$$

With k=1, a spatial component is now introduced and once again the solute transport equation can be integrated through space.

$$\iiint_{-\infty}^{\infty} x\frac{\partial}{\partial t}(nC)dxdydz = \frac{\partial}{\partial t}\iiint_{-\infty}^{\infty} xnC \; dxdydz = \frac{dM_{1x}}{dt} \tag{2.11.1}$$

$$\iiint_{-\infty}^{\infty} x\frac{\partial}{\partial t}(\rho_b S)dxdydz = \rho_b\frac{\partial}{\partial t}\iiint_{-\infty}^{\infty} xS \; dxdydz \tag{2.11.2}$$

$$\iiint_{-\infty}^{\infty} -x\frac{\partial}{\partial x}(q_x C)dxdydz = -\iint_{-\infty}^{\infty} dydz \int_{-\infty}^{\infty} x\frac{\partial}{\partial x}(q_x C)dx \tag{2.11.3}$$

$$= -\iint_{-\infty}^{\infty} dydz\,[-\int q_x C\,dx]_{-\infty}^{\infty}$$

Combining the final two integrals in the above equation yields

$$q_x \iiint_{-\infty}^{\infty} C\,dxdydz = \frac{q_x}{n}M_0 = V_x M_0 \tag{2.11.4}$$

Analyzing q_y by the same methodology shows that

$$\iiint_{-\infty}^{\infty} -x\frac{\partial}{\partial y}(q_y C)dxdydz = -\iint_{-\infty}^{\infty} xdxdz \int_{-\infty}^{\infty} \frac{\partial}{\partial y}(q_y C)dy \tag{2.11.5}$$

$$= -\iint_{-\infty}^{\infty} xdxdz\,[q_y C]_{-\infty}^{\infty} = 0$$

By the same analysis we can see that for q_z

$$\iiint_{-\infty}^{\infty} -x\frac{\partial}{\partial z}(q_z C)dxdydz = 0 \tag{2.11.6}$$

The third term in the solute transport equation can now be integrated through space

$$\iiint_{-\infty}^{\infty} (x\frac{\partial}{\partial x_i}[n\,D_{ij}\frac{\partial C}{\partial x_j}])\,dxdydz = \iint_{-\infty}^{\infty} dydz \int_{-\infty}^{\infty} (x\frac{\partial}{\partial x_i}[n\,D_{ij}\frac{\partial C}{\partial x_j}])dx \tag{2.11.7}$$

Integrating with respect to x first shows that

$$\iint_{-\infty}^{\infty} dydz \int_{-\infty}^{\infty} x\frac{\partial}{\partial x}\left[nD_{xx}\frac{\partial C}{\partial x}\right]dx \tag{2.11.8}$$

$$= \iint_{-\infty}^{\infty} dydz \ [xnD_{xx}\frac{\partial C}{\partial t} - \int nD_{xx}\frac{\partial C}{\partial t}dx]_{-\infty}^{\infty} = 0$$

Following the same method for y and z yields

$$\iiint_{-\infty}^{\infty} (x\frac{\partial}{\partial y}[D_{yy}\frac{\partial C}{\partial y}])\ dxdydz \ and \iiint_{-\infty}^{\infty} (x\frac{\partial}{\partial z}[D_{zz}\frac{\partial C}{\partial z}])\ dxdydz = 0 \tag{2.11.9}$$

Combining the three previous solutions and applying the same process for the x and y components of the first spatial moment yield a differential equation for the changes in the center of mass of a groundwater plume over time.

$$\frac{dM_{1x}}{dt} + \rho_b\frac{\partial}{\partial t}\iiint_{-\infty}^{\infty} xS\ dx\ dy\ dz = V_x M_0 \tag{2.12.1}$$

$$\frac{dM_{1y}}{dt} + \rho_b\frac{\partial}{\partial t}\iiint_{-\infty}^{\infty} yS\ dx\ dy\ dz = V_y M_0 \tag{2.12.2}$$

$$\frac{dM_{1z}}{dt} + \rho_b\frac{\partial}{\partial t}\iiint_{-\infty}^{\infty} zS\ dx\ dy\ dz = V_z M_0 \tag{2.12.3}$$

2.2.3 Manipulation of the Solute Transport Equation (Second Moment)

The second spatial moment can now be evaluated with k=2.

$$x^2\frac{\partial}{\partial t}(nC + \rho_b S) = -x^2\frac{\partial}{\partial x_i}(q_i C) + x^2\frac{\partial}{\partial x_i}[D_{ij}\frac{\partial C}{\partial x}] \tag{2.13}$$

Integrating the solute transport equation unique for the second spatial moment through space and by parts leads to

$$\iiint_{-\infty}^{\infty} x^2\frac{\partial}{\partial t}(nC)dxdydz = \frac{\partial}{\partial t}\iiint_{-\infty}^{\infty} x^2 nC\ dxdydz = \frac{dM_{2x}}{dt} \tag{2.14.1}$$

$$\iiint_{-\infty}^{\infty} x^2 \frac{\partial}{\partial t}(\rho_b S)dxdydz = \rho_b \frac{\partial}{\partial t}\iiint_{-\infty}^{\infty} x^2 S\, dxdydz \tag{2.14.2}$$

$$\iiint_{-\infty}^{\infty} -x^2 \frac{\partial}{\partial x}(q_x C)dxdydz = -\iint_{-\infty}^{\infty} dydz \int_{-\infty}^{\infty} x^2 \frac{\partial}{\partial x}(q_x C)dx \tag{2.14.3}$$

$$= -\iint_{-\infty}^{\infty} dydz\,[-2\int x\, q_x C\, dx]_{-\infty}^{\infty}$$

Combining the final two integrals in the above equation yields

$$2\, q_x \iiint_{-\infty}^{\infty} x\ C\, dxdydz = \frac{2q_x}{n} M_{1x} = 2V_x M_{1x} \tag{2.14.4}$$

Once again we can analyze q_y and q_z by the same methodology

$$\iiint_{-\infty}^{\infty} -x^2 \frac{\partial}{\partial y}(q_y C)dxdydz = -\iint_{-\infty}^{\infty} x^2 dxdz \int_{-\infty}^{\infty} \frac{\partial}{\partial y}(q_y C)dy \tag{2.14.5}$$

$$= -\iint_{-\infty}^{\infty} x^2 dxdz\ [q_y C]_{-\infty}^{\infty} = 0$$

By the same analysis it can be seen that

$$\iiint_{-\infty}^{\infty} -x^2 \frac{\partial}{\partial z}(q_z C)dxdydz = 0 \tag{2.14.6}$$

Integrating the third term in the solute equation yields

$$\iiint_{-\infty}^{\infty} (x^2 \frac{\partial}{\partial x_i}[n\, D_{ij} \frac{\partial C}{\partial x_j}])\, dxdydz = \iint_{-\infty}^{\infty} dydz \int_{-\infty}^{\infty} (x^2 \frac{\partial}{\partial x_i}[n\, D_{ij} \frac{\partial C}{\partial x_j}])dx \tag{2.14.7}$$

After integrating through by parts we obtain

$$\iint_{-\infty}^{\infty} dydz \int_{-\infty}^{\infty} x^2 \frac{\partial}{\partial x}\left[n\, D_{xx} \frac{\partial C}{\partial x}\right] dx \tag{2.14.8}$$

$$= \iint_{-\infty}^{\infty} dydz \; [x^2\, n\, D_{xx} \frac{\partial C}{\partial t} - 2 \int x\, n\, D_{xx} \frac{\partial C}{\partial t} dx]_{-\infty}^{\infty}$$

$$= -2\, n\, D_{xx} \iint_{-\infty}^{\infty} dydz \int_{-\infty}^{\infty} x\, \frac{\partial C}{\partial x} dx \tag{2.14.9}$$

$$= -2\, n\, D_{xx} \iint_{-\infty}^{\infty} dydz \; [\, x\, C - \int C\, dx]_{-\infty}^{\infty}$$

$$= 2\, D_{xx} \iiint_{-\infty}^{\infty} n\, C\, dxdydz = 2\, D_{xx}\, M_0 \tag{2.14.10}$$

At high order moments, the local dispersion terms must also be evaluated. Here D_{yy} is analyzed,

$$\iiint_{-\infty}^{\infty} (\, x^2 \frac{\partial}{\partial y}[D_{yy} \frac{\partial C}{\partial y}])\, dxdydz = \iint_{-\infty}^{\infty} x^2\, dxdz \int_{-\infty}^{\infty} \frac{\partial}{\partial y}\left[D_{yy} \frac{\partial C}{\partial y}\right] dy = 0 \tag{2.14.11}$$

Therefore by the same analysis we can find that for D_{zz}

$$\iiint_{-\infty}^{\infty} (\, x^2 \frac{\partial}{\partial z}[D_{zz} \frac{\partial C}{\partial z}])\, dxdydz = 0 \tag{2.14.12}$$

Combining all solutions into differentials for the second spatial moment it can be seen that changes in the variance about the center of mass of a ground water plume is dependent upon the velocity in the given direction, the first spatial moment, and the local dispersion term.

$$\frac{dM_{2x}}{dt} + \rho_b \frac{\partial}{\partial t} \iiint_{-\infty}^{\infty} x^2 S \, dx \, dy \, dz = 2V_x M_{1x} + 2D_{xx} M_0 \tag{2.15.1}$$

$$\frac{dM_{2y}}{dt} + \rho_b \frac{\partial}{\partial t} \iiint_{-\infty}^{\infty} y^2 S \, dx \, dy \, dz = 2V_y M_{1y} + 2D_{yy} M_0 \tag{2.15.2}$$

$$\frac{dM_{2z}}{dt} + \rho_b \frac{\partial}{\partial t} \iiint_{-\infty}^{\infty} z^2 S \, dx \, dy \, dz = 2V_z M_{1z} + 2D_{zz} M_0 \tag{2.15.3}$$

2.2.4 Zeroth Moment Mathematical Derivation

Using the derived equation for total mass in solution, a relationship can be used that relates the amount of sorbed mass to the mass in solution by a Freundlich constant, K_F, which notes the likelihood of a solute to adsorb to soil, and a dimensionless exponential adsorption coefficient, N. Taking the integral through space and applying previously derived equations, the time dependent changes of spatial moments can be derived.

$$\iiint_{-\infty}^{\infty} {x_i}^k S \, dx \, dy \, dz = K_F \iiint_{-\infty}^{\infty} {x_i}^k C^N \, dx \, dy \, dz \tag{2.16}$$

A Gaussian Plume approximation, which assumes that as a solute plume propagates through the ground it remains Gaussian in shape, is used to simplify the integration. The Gaussian approximation for a three-dimensionally moving plume is defined below. This approximation can then be substituted into Equation 2.16 and integrated over time.

$$C(x,y,z,t) = \frac{M_0 \, e^{-\frac{(x-V_x t)^2}{4D_{11}t} - \frac{(y-V_y t)^2}{4D_{22}t} - \frac{(z-V_z t)^2}{4D_{33}t}}}{n \, (4\pi D_{11} t)^{1/2} (4\pi D_{22} t)^{1/2} (4\pi D_{33} t)^{1/2}} \tag{2.17}$$

Defining a constant, A, and making use of U-Substitutions, the Gaussian Approximation can be simplified further to provide easier integration.

$$A = [\frac{M_0}{n\ (4\pi D_{11}t)^{1/2}(4\pi D_{22}t)^{1/2}(4\pi D_{33}t)^{1/2}}]^N \tag{2.18.1}$$

$$U_1 = \frac{N^{\frac{1}{2}}(x - V_x t)}{(4D_{11}t)^{\frac{1}{2}}} \qquad dx = (\frac{4D_{11}t}{N})^{\frac{1}{2}} dU_1 \tag{2.18.2}$$

$$U_2 = \frac{N^{\frac{1}{2}}(y - V_y t)}{(4D_{22}t)^{\frac{1}{2}}} \qquad dy = (\frac{4D_{22}t}{N})^{\frac{1}{2}} dU_2 \tag{2.18.3}$$

$$U_3 = \frac{N^{\frac{1}{2}}(z - V_z t)}{(4D_{33}t)^{\frac{1}{2}}} \qquad dz = (\frac{4D_{33}t}{N})^{\frac{1}{2}} dU_3 \tag{2.18.4}$$

$$K_F \iiint_{-\infty}^{\infty} C^N\, dx\, dy\, dz \tag{2.19}$$

$$= K_F A (\frac{4D_{11}t}{N})^{\frac{1}{2}} (\frac{4D_{22}t}{N})^{\frac{1}{2}} (\frac{4D_{33}t}{N})^{\frac{1}{2}} \iiint_{-\infty}^{\infty} e^{-U_1^2 - U_2^2 - U_3^2}\ dU_1 dU_2 dU_3$$

The triple integral works out perfectly to a total of $\pi^{3/2}$ and can then be substituted into Equation 2.9 for M_s, or total mass adsorbed.

$$M_0 + \rho_b K_F A \pi^{\frac{3}{2}} \left(\frac{4D_{11}t}{N}\right)^{\frac{1}{2}} \left(\frac{4D_{22}t}{N}\right)^{\frac{1}{2}} \left(\frac{4D_{33}t}{N}\right)^{\frac{1}{2}} = M_T \tag{2.20}$$

Rearranging terms and substituting for A leads to

$$M_0 + \frac{\rho_b K_F {M_0}^N}{N^{\frac{3}{2}}\, n^N} [(4\pi D_{11}t)(4\pi D_{22}t)(4\pi D_{33}t)]^{\frac{1-N}{2}} = M_T \tag{2.21}$$

Defining a new constant, B, allows for simplification of Equation 2.21.

$$B = \frac{\rho_b K_F}{N^{\frac{3}{2}} n^N}[(4\pi D_{11})(4\pi D_{22})(4\pi D_{33})]^{\frac{1-N}{2}} \tag{2.22}$$

Substituting in B to Equation 2.21 and dividing through by M_T gives the relationship of the mass in solution to the total mass. It can be seen from the equation below that at the initial time, t=0, the ratio of mass in solution to total mass is equal to 1 which verifies the previously derived equations on a mathematical basis.

$$\frac{M_0}{M_T} + \frac{B}{{M_T}^{1-N}}(\frac{M_0}{M_T})^N t^{\frac{3}{2}(1-N)} = 1 \tag{2.23}$$

2.2.5 First Moment Mathematical Derivation

The first spatial moment relationship can now be derived with k=1 in Equation 2.16

$$\iiint_{-\infty}^{\infty} xS\,dx\,dy\,dz = K_F \iiint_{-\infty}^{\infty} xC^N\,dx\,dy\,dz \tag{2.24}$$

Using the same technique that was used for deriving the zeroth moment, the first moment can be easily derived.

$$K_F \iiint_{-\infty}^{\infty} xC^N\,dx\,dy\,dz \tag{2.25}$$

$$= K_F A(\frac{4D_{11}t}{N})^{\frac{1}{2}}(\frac{4D_{22}t}{N})^{\frac{1}{2}}(\frac{4D_{33}t}{N})^{\frac{1}{2}} \iiint_{-\infty}^{\infty} xe^{-{U_1}^2-{U_2}^2-{U_3}^2}\,dU_1 dU_2 dU_3$$

Including the new (x,y,z) component into the calculation complicates this slightly and adds an additional step

$$K_F A(\frac{4D_{11}t}{N})^{\frac{1}{2}}(\frac{4D_{22}t}{N})^{\frac{1}{2}}(\frac{4D_{33}t}{N})^{\frac{1}{2}} \int_{-\infty}^{\infty} e^{-{U_2}^2}dU_2 \int_{-\infty}^{\infty} e^{-{U_3}^2}dU_3 \int_{-\infty}^{\infty} xe^{-{U_1}^2}dU_1 \tag{2.26}$$

The first two integrals lead to the square root of π while the final integral leads to

$$\int_{-\infty}^{\infty} \left[\left(\frac{4D_{11}t}{N}\right)^{\frac{1}{2}} U_1 + V_x t\right] e^{-{U_1}^2} dU_1 = V_x t \int_{-\infty}^{\infty} e^{-{U_1}^2} dU_1 \tag{2.27}$$

Combining the previous answer with the answers from the previous line yield

$$\frac{\rho_b K_F {M_0}^N}{N^{\frac{3}{2}} n^N} [(4\pi D_{11}t)(4\pi D_{22}t)(4\pi D_{33}t)]^{\frac{1-N}{2}} V_x t \tag{2.28}$$

Recalling from earlier derivations that the solute transport equation was found to be the equation below, the triple integral can now be replaced with what has just been derived.

$$\frac{dM_{1x}}{dt} + \rho_b \frac{\partial}{\partial t} \iiint_{-\infty}^{\infty} xS\, dx\, dy\, dz = V_x M_0 \tag{2.12.1}$$

$$\frac{dM_{1x}}{dt} + \frac{\rho_b K_F}{N^{\frac{3}{2}} n^N} [(4\pi D_{11})(4\pi D_{22})(4\pi D_{33})]^{\frac{1-N}{2}} V_x \frac{d}{dt}\left[{M_0}^N t^{\frac{5-3N}{2}}\right] = V_x M_0 \tag{2.29.1}$$

Taking the time derivative of the last term on the left side of Equation 2.29.1 leads to

$$\frac{d}{dt}\left[{M_0}^N t^{\frac{5-3N}{2}}\right] = N{M_0}^{N-1} t^{\frac{5-3N}{2}} \frac{dM_0}{dt} + \frac{5-3N}{2} {M_0}^N t^{\frac{3-3N}{2}} \tag{2.29.2}$$

Find the time derivative of the zeroth moment leads to

$$M_0 + B{M_0}^N t^{\frac{3-3N}{2}} = M_T \tag{2.29.3}$$

$$\frac{dM_0}{dt} + NB{M_0}^{N-1} t^{\frac{3-3N}{2}} \frac{dM_0}{dt} + \frac{3-3N}{2} B{M_0}^N t^{\frac{1-3N}{2}} = 0 \tag{2.29.4}$$

$$\frac{dM_0}{dt}\left[1 + NB{M_0}^{N-1} t^{\frac{3-3N}{2}}\right] = -\frac{3-3N}{2} B{M_0}^N t^{\frac{1-3N}{2}} \tag{2.29.5}$$

$$\frac{dM_0}{dt} = \frac{-\frac{3-3N}{2} B{M_0}^N t^{\frac{1-3N}{2}}}{1 + NB{M_0}^{N-1} t^{\frac{3-3N}{2}}} \tag{2.29.6}$$

Substituting back into Equation 52, the time derivatives of the first spatial moment can be found in the (x,y,z) coordinate system. To proceed with solving the time derivate of the first spatial moment, backwards Euler integration is needed in order to solve the integration.

$$\frac{dM_{1x}}{dt} = V_x M_0 - V_x B[\frac{5-3N}{2} {M_0}^N t^{\frac{3-3N}{2}} - \frac{\frac{3}{2}(N-N^2)B{M_0}^{2N-1}t^{3-3N}}{1+ NB{M_0}^{N-1}t^{\frac{3-3N}{2}}}] \quad (2.30.1)$$

$$\frac{dM_{1y}}{dt} = V_y M_0 - V_y B[\frac{5-3N}{2} {M_0}^N t^{\frac{3-3N}{2}} - \frac{\frac{3}{2}(N-N^2)B{M_0}^{2N-1}t^{3-3N}}{1+ NB{M_0}^{N-1}t^{\frac{3-3N}{2}}}] \quad (2.30.2)$$

$$\frac{dM_{1z}}{dt} = V_z M_0 - V_z B[\frac{5-3N}{2} {M_0}^N t^{\frac{3-3N}{2}} - \frac{\frac{3}{2}(N-N^2)B{M_0}^{2N-1}t^{3-3N}}{1+ NB{M_0}^{N-1}t^{\frac{3-3N}{2}}}] \quad (2.30.3)$$

Chapter 3: Results

3.1 Field Data Comparison

By using the method described in section 2.1, spatial moment analysis can be conducted for the data from the field experiment. These values can be compared to those of Garabedian 1987 in which a similar approach to calculate spatial moments was applied.

3.1.1 Lithium Data

Below, in Table 1, a comparison of the zeroth, first, and second moments of lithium can be seen between this study and the Garabedian 1987 study. Small variations in zeroth moment calculations arise due to changes in triangulation schemes performed. These changes are slightly compounded at higher moments, thus leading to small variations between studies for the first and second spatial

moments. For the zeroth moment calculation, there is an average percentage change of +8.5% when comparing this study to that of Garabedian, however when the values from day 111 are considered there is only a +6% increase in values. The author has decided that the values from day 111 in the Garabedian study may be an erroneous outlier, thus allowing for the exclusion in the difference calculation.

Table 1.

Lithium Zeroth Moment (Concentration (g))			
Days after Injection	Garabedian	Current Study	Percentage Change
13	366	380.60	3.99
33	415	414.83	-0.04
55	343	341.36	-0.48
83	248	248.52	0.21
111	158	234.84	48.63
139	186	190.40	2.37
174	108	138.80	28.52
203	144	166.13	15.37
237	121	130.99	8.26
273	89	94.47	6.15
315	65	67.95	4.54
349	60	61.33	2.22
384	67	70.82	5.70
426	26	25.98	-0.08
461	56	63.84	14.00
511	61	63.36	3.87
657	37	37.47	1.27

Looking to the comparisons for the first and second moments in Tables 2 and 3 respectively, it can be seen that the values derived from this study compare very well to those of Garabedian. There once again seems to be an erroneous value for the final observation of the Garabedian values, as the first moment, the location of the center of mass, actually becomes closer to the site of injection by 70 feet in the y-direction. As with the zeroth moment values, the author believes this value can be regarded as a potential calculation error. The movement of the Lithium plume is predominantly in the negative y direction, as can be seen from the first moment data. Difference in the y position of the center of mass, after removing the final day

of data, leads to a difference of 1.8% between studies. The second moment data shows very similar differences between studies with only a 0.38% difference after a potential erroneous data point is ignored on the 111th day.

Table 2.

Lithium First Moment Comparison (Center of Mass Location (ft))						
Garabedian Study				Current Study		
X	Y	Z	Days after Injection	X	Y	Z
1.9	-19.5	40.2	13	1.7	-19.7	40.2
6.7	-43.7	39.2	33	6.5	-43.5	39.2
7.7	-64.7	37.7	55	7.4	-64.5	37.7
13.5	-91.5	37.0	83	13.1	-91.3	37.0
21.6	-136.3	36.6	111	19.8	-121.5	36.6
22.9	-147.5	36.3	139	23.2	-147.1	36.3
26.0	-172.3	36.1	174	24.6	-160.5	36.2
26.4	-183.7	35.3	203	25.7	-178.2	35.3
26.1	-196.0	34.7	237	25.8	-192.7	34.8
25.4	-195.9	34.7	273	25.2	-191.6	34.7
27.8	-205.7	34.8	315	27.9	-204.3	34.8
31.2	-226.4	34.5	349	31.4	-225.9	34.5
28.7	-205.7	34.7	384	28.9	-202.9	34.7
37.7	-281.3	33.6	426	37.6	-281.2	33.6
30.2	-223.2	34.3	461	30.1	-221.6	34.4
30.4	-234.9	33.9	511	30.1	-230.9	34.0
36.3	-163.5	33.4	657	36.3	-263.6	33.4

Table 3.

Lithium Second Moment Comparison (Variance (ft^2))						
Garabedian Study				Current Study		
X	Y	Z	Days after Injection	X	Y	Z
17.4	43.5	4.71	13	12.5	39.3	4.7
17.6	117.4	5.25	33	13.4	109.1	5.2
17.2	222.3	4.95	55	13.4	217.3	4.8
17.8	412.2	4.72	83	14.7	402.0	4.6
19.8	239.2	3.28	111	16.8	783.1	4.3
19.5	1057.0	5.17	139	11.2	1046.8	4.9
17.6	1790.0	5.31	174	12.7	2049.5	5.2
48.0	1843.0	6.50	203	13.8	2094.0	6.4
40.7	2272.0	6.98	237	26.3	2448.1	6.7
29.0	2934.0	7.46	273	19.3	2934.9	7.2
29.7	5318.0	7.18	315	18.5	5097.6	6.9
26.7	3711.0	7.14	349	15.4	3752.6	6.6
28.0	4544.0	7.18	384	20.4	4538.6	6.5
28.8	2149.0	4.00	426	15.6	2160.1	3.5
32.1	5652.0	7.46	461	19.7	5588.6	7.0
32.0	5482.0	7.84	511	20.4	5372.3	7.4
23.7	8452.0	7.34	657	11.3	8315.0	6.9

Below in Figures 5-7 a linear comparison is made for the zeroth, first, and second spatial moments between this study and that of Garabedian. For the zeroth moment, a slope of 0.9995 and an R^2 value of 0.976 is found in the comparison.

Looking to the first moment, a slope of 0.9921 and an R^2 value of 0.8886 are found. When the erroneous point on the last sampling day is removed, the resulting slope and R^2 are 0.9930 and 0.9966 respectively. Finally for the second moment, the slope is 0.9625 and R^2 is 0.9958. Once again the erroneous point on day 111 can be removed and the resulting slope and R^2 are 0.9745 and 0.9978 respectively.

Figure 5.

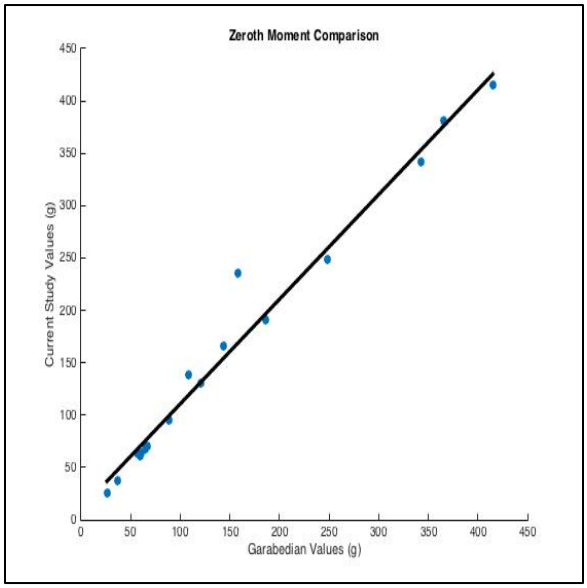

Figure 6.

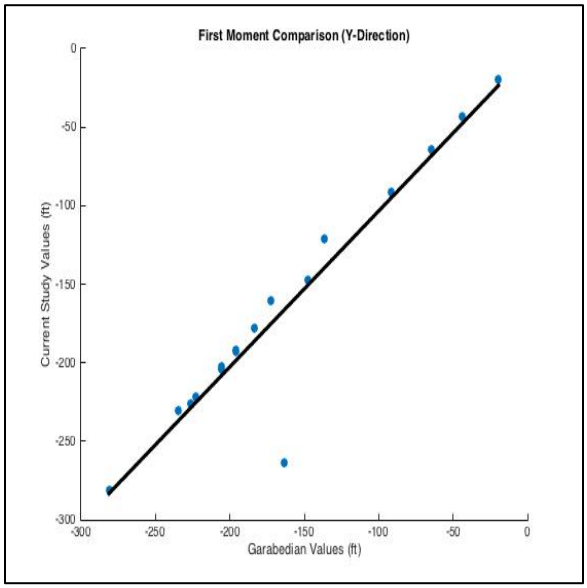

Figure 7.

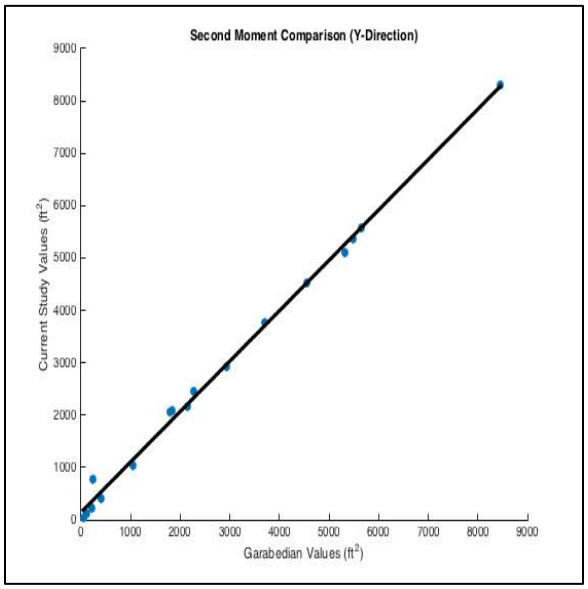

3.1.2 Bromide Data

A quick look at the data for bromide can provide a comparison to the lithium data and the ability to show the differences between substances that undergo sorption those that do not. Bromide data from the Cape Cod site has been studied extensively when compared to that of lithium (Garabedian 1987, Garabedian et al. 1991a, LeBlanc et al. 1991). In Tables 4-6, comparisons between the spatial moments of bromide from this study and the Garabedian 1987 study are shown. It can be seen that as was the case with lithium, the values for both studies are very close. The fact that bromide does not undergo adsorption is evident from the lack of a decrease in the zeroth moment values. This can be shown mathematically by looking to Equation 2.9 and noticing that in the absence of sorption M_s will always be equal to 0, thus making the mass in solution being equal to the total mass. The distance traveled by the bromide plume over the duration of the study can also be seen to be higher than that of the lithium as no retardation of the flow occurs due to

the overall lack of sorption. Finally, the variance shows lower values during the later stages of the experiment as the plume spreads less than that of lithium. The spreading that results in the lithium case rather than the bromide case is due to the sorption process leaving mass behind as the groundwater plume moves southward. When bromide is considered, the lack of sorption leads to the plume staying together throughout the tracer test and therefore reducing the spread of the plume, which is seen in the second moment data.

Table 4.

Bromide Zeroth Moment Comparison (Concentration (g))			
Days After Injection	Garabedian	Current Study	Percentage Change
13	4442	4234.00	4.68
33	5146	4746.00	7.77
55	4939	4286.00	13.22
83	4986	4890.00	1.93
111	4912	4783.00	2.63
139	4229	4301.00	-1.70
174	4318	4245.00	1.69
203	4850	4527.00	6.66
237	4901	4862.00	0.80
273	4469	4667.00	-4.43
315	4808	4777.00	0.64
349	4916	4762.00	3.13
384	4927	4870.00	1.16
426	4936	4970.00	-0.69
461	4998	5104.00	-2.12
511	4953	4303.00	13.12

Table 5.

Bromide First Moment Comparison (Center of Mass Location (ft))						
Garabedian				Current Study		
X	Y	Z	Days after Injection	X	Y	Z
2.5	-24.3	40.3	13	2.0	-23.0	39.9
8.7	-55.3	38.3	33	7.6	-52.9	38.0
9.9	-85.0	36.3	55	8.7	-80.4	35.8
18.5	-127.6	34.7	83	18.6	-128.7	35.1
26.7	-167.1	33.8	111	27.3	-168.2	34.1
33.2	-211.5	33.9	139	32.9	-209.2	33.8
36.5	-251.2	31.6	174	37.0	-255.2	32.0
37.5	-291.4	30.8	203	38.1	-285.9	31.1
38.6	-329.3	30.3	237	39.4	-324.2	30.5
43.5	-375.0	30.2	273	43.0	-375.2	29.9
54.8	-439.4	30.8	315	54.9	-439.2	30.9
62.4	-483.8	30.7	349	62.0	-479.9	30.5
71.7	-532.7	30.3	384	71.9	-534.4	30.2
83.2	-592.0	29.3	426	83.0	-591.9	29.3
93.7	-644.1	28.6	461	93.9	-643.9	28.6
106.3	-702.1	26.6	511	100.5	-687.6	26.1

Table 6.

Bromide Second Moment Comparison (Variance (ft^2))						
Garabedian Study				Current Study		
X	Y	Z	Days after Injection	X	Y	Z
16.6	69.8	4.0	13	10.9	45.8	4.0
19.8	217.1	5.0	33	16.3	139.8	4.9
20.7	375.1	5.4	55	16.6	218.3	4.7
26.7	564.5	7.8	83	21.8	564.5	5.6
33.8	921.5	7.9	111	23.6	906.1	7.1
37.4	1261.1	7.7	139	26.0	1336.7	7.3
46.3	1443.5	11.1	174	34.5	1518.1	8.8
41.4	1742.0	11.0	203	28.1	2206.6	10.0
54.7	1910.4	11.3	237	56.4	2856.1	12.0
55.8	2114.4	11.3	273	50.0	2087.7	10.4
65.0	2590.2	14.7	315	60.5	2673.9	14.5
63.2	2441.1	9.4	349	55.6	2837.0	10.1
75.0	3515.7	8.8	384	67.5	3532.1	7.6
82.8	3597.1	8.7	426	70.8	3577.6	7.9
76.9	4003.2	10.5	461	57.2	3992.0	8.8
112.5	4362.9	14.3	511	84.2	3257.3	13.8

3.2 Quantitative Modeling

Using the quantitative models derived in section 2.2, comparisons can now be made between the values shown in the tables above and those derived from the model.

3.2.1 Zeroth Moment

Using Equation 2.23, the ratio of mass in solution, the zeroth moment, to the total mass can be solved for and then modeled against that of the field data that has been shown in section 3.1. Values for some state variables are listed in Table 7. All values have been taken from Miralles-Wilhelm 1993.

Table 7.

Defined Values	
M_T	595 g
D_{11}	11000 cm^2/day
D_{22}	22 cm^2/day
D_{33}	.22 cm^2/day
K_F	0.3 $(l/mg)^{0.5}$
ρ_b	1.7 g/cm^3
n	0.39
N	0.5

What is expected is that the quantitative modeling equation, Equation 2.23, will match the structure of the field data. Figure 8 below shows the comparison

between the modeled equation, line, and the field data, circles. It can be seen that the match is nearly identical when comparing the two and thus the author believes that with the help of simple governing equations and a few approximations, the zeroth moment of a nonlinear sorbing solute can be traced through time using Equation 2.23. Slight modifications have been made to fit the line to the field data. In order to better fit the modeled line to the data, a trial and error adjustment of the adsorption coefficient and Freundlich coefficient have been made by slightly changing each value until an acceptable fit was reached. By keeping both the adsorption coefficient and Freundlich coefficient close to the estimated values from Garabedian, it is ensured that the model is not changing the overall dynamics of the aquifer.

Figure 8.

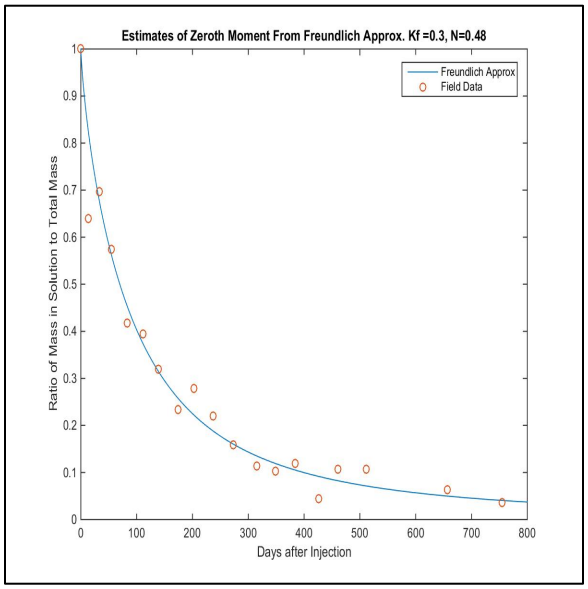

3.2.2 First and Second Moments

Graphical representations of the first and second moments values in the y-direction are shown in Figures 9 and 10 respectively. Values in both plots for day 426 show unexpected decreases, which has been noted as an incomplete sampling day (Garabedian 1987). During modeling of the first and second moments, the data point for day 426 will be ignored for better representation of true plume characteristics. The relative velocity of the lithium plume can be interpreted by looking to the slope of the blue line in Figure 9 and can be seen slowing down during the second half of the experiment, especially when compared to the red line which represents the movement of the bromide plume. The relative speed of the bromide plume remains close to constant throughout the experiment as it moves with the groundwater. As the velocity of lithium slows down in Figure 9, the variance of lithium, blue line, in Figure 10 continues to increase as sorption continues to increase the spread of the plume. Meanwhile the bromide plume does not show as great of a variance towards the end of the experiment when compared to lithium as shown in Section 3.1.2

Figure 9.

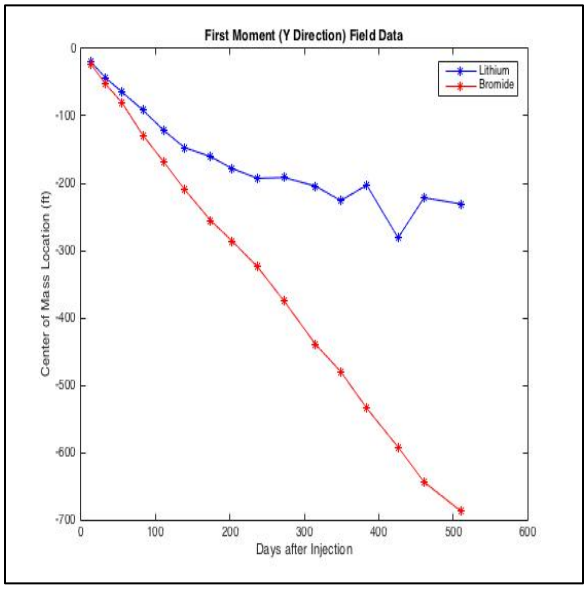

Figure 10.

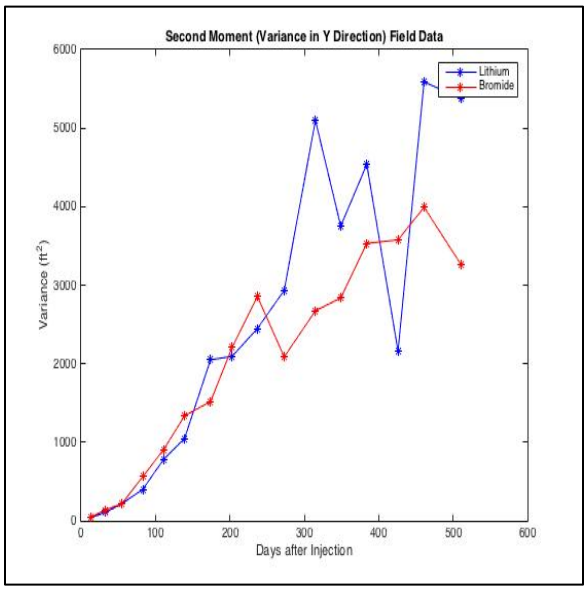

An attempt was made at modeling the first spatial moment by solving Equation 2.30.1 through the use of backwards Eularian integration. It was found that the model projected an overall acceleration of the center of mass throughout

the duration of the experiment, which when looking at Figures 4 and 9, it can be seen that the plume itself slows down compared to that of the overall groundwater velocity. Theories as to why the zeroth moment works well and the first moment does not are limited, but the author notes that the Gaussian approximation may not be appropriate nonlinear sorption as the plume in Figure 4, losing the Gaussian features very early in the experiment.

Chapter 4: Summary and Conclusion

4.1 Summary

Through the use of trapezoidal integration and Delaunay triangulation, spatial moment calculations have been made for a nonlinear sorbing solution of lithium at the Cape Cod tracer test. These values have shown to be comparable to a prior study completed by Garabedian 1987 with R^2 values all near or greater than 90%. With confirmed calculations of spatial moments from field data, derivations of quantitative models of spatial moments could be made using a Gaussian Plume model approximation as well as having aquifer specific porosity and hydraulic conductivity.

The quantitative representation of the zeroth moment has shown to match up extremely well with that of the field data calculated prior. With the flexibility of being able to tweak the adsorption coefficient as well as the Freundlich coefficient to allow the model of the zeroth moment to match the field data provides a powerful tool if both values remain logical. The values used for the adsorption coefficient and Freundlich coefficient have been estimated from previous studies(Garabedian 1987;

Miralles-Wilhelm 1993) and while they have been slightly for this study, the changes allow the values to remain within reason.

4.2 Improvements

Quantitative models of higher moments currently are unsolvable due to the first assumption made for this study. By using a Gaussian Plume approximation, it has been assumed that as the contamination plume travels, the plume remains Gaussian in nature throughout the duration of the test. From Figure 4, it can be seen that the lithium plume loses the Gaussian form the longer the test lasts as there is sorption taking place as the plume moves and the spread of the plume increases in the y-direction. In order to solve for the higher moments an approach that does not utilize the Gaussian approximation may be necessary. In addition to correcting the plume approximation, improvements can be made in the comparison to the Garabedian moment analysis. The author has disregarded several days of records when comparing calculations of the spatial moments, however, investigations into the differences may be warranted, as the differences do not fall on one specific sampling date.

4.3 Future Work

With the successful derivation of the zeroth moment model, successfully solving for higher moments would be the next step. Stochastic analysis was attempted in order to account for small deviations in state variables throughout the duration of the experiment, however the resulting analysis revealed that all significant quantities were too small in the result. Adapting the stochastic approach from works such as Gelhar 1993 and Miralles-Wilhelm and Gelhar 1996 may lead to

solutions that correctly solve the first moment, but only after the Gaussian approximation is addressed.

References

Bürgisser, Christa S., et al. "Determination of nonlinear adsorption isotherms from column experiments: An alternative to batch studies." Environmental Science & Technology 27.5 (1993): 943-948.

Delaunay, Boris. "Sur la sphere vide." Izv. Akad. Nauk SSSR, Otdelenie Matematicheskii i Estestvennyka Nauk 7.793-800 (1934): 1-2.

Freundlich, U. "Die adsorption in lusungen." (1906): 385-470.

Garabedian, Stephen P. Large-scale dispersive transport in aquifers: Field experiments and reactive transport theory. Diss. Massachusetts Institute of Technology, 1987.

Garabedian, Stephen P., and Damus R. LEBLANC. "2. Analysis of Spatial Moments for a Nonreactive Tracer." Water Resources Research 27.5 (1991): 911-924.

Gelhar, Lynn W. Stochastic subsurface hydrology. Prentice-Hall, 1993.

Miralles-Wilhelm, Fernando. Stochastic analysis of sorption and biodegradation in three-dimensionally heterogeneous aquifers. Diss. Massachusetts Institute of Technology, 1993.

Miralles‐Wilhelm, F., and L. W. Gelhar. "Stochastic analysis of sorption macrokinetics in heterogeneous aquifers." Water resources research 32.6 (1996): 1541-1549.

LeBlanc, Denis R., et al. "Large‐scale natural gradient tracer test in sand and gravel, Cape Cod, Massachusetts: 1. Experimental design and observed tracer movement." Water Resources Research 27.5 (1991): 895-910.

Sudicky, Edward A. "A natural gradient experiment on solute transport in a sand aquifer: Spatial variability of hydraulic conductivity and its role in the dispersion process." Water Resources Research 22.13 (1986): 2069-2082.

Wood, David Muir. Soil behaviour and critical state soil mechanics. Cambridge university press, 1990.